Nanoscale Res Lett (2007) 2:405–409
DOI 10.1007/s11671-007-9075-3

NANO EXPRESS

Tungsten Oxide Nanorods Array and Nanobundle Prepared by Using Chemical Vapor Deposition Technique

X. P. Wang · B. Q. Yang · H. X. Zhang · P. X. Feng

Received: 16 May 2007 / Accepted: 15 June 2007 / Published online: 7 July 2007

Abstract Tungsten oxide (WO_3) nanorods array prepared using chemical vapor deposition techniques was studied. The influence of oxygen gas concentration on the nanoscale tungsten oxide structure was observed; it was responsible for the stoichiometric and morphology variation from nanoscale particle to nanorods array. Experimental results also indicated that the deposition temperature was highly related to the morphology; the chemical structure, however, was stable. The evolution of the crystalline structure and surface morphology was analyzed by scanning electron microscopy, Raman spectra and X-ray diffraction approaches. The stoichiometric variation was indicated by energy dispersive X-ray spectroscopy and X-ray photoelectron spectroscopy.

Keywords Nanostructure · Tungsten oxide · Nanorod · Nanobundle · CVD

Introduction

Nanostructured transition metal oxides are outstanding candidates for a wide range of applications including lithium-ion batteries, [1, 2] catalysts, [3] electrochromic materials, [4, 5] and sensors. [6, 7] Nanostructured tungsten oxide, as a typical transition metal oxide material, has been researched frequently these years.

The nanostructured tungsten oxide material exhibited many excellent properties because of their particular phase structure and huge surface areas, which depend greatly on the experimental parameters. In previous experiment of chemical vapor deposition (CVD), it was realized that several factors, such as filament temperature, electrical current, gas flow and the composition of gas, would affect the structure of the sample. The major factors could be the substrate temperature and the chamber pressure [8]. Moreover, the effect of the reaction gas concentration on the sample properties was also preliminarily studied [9].

Based on the previous achievements, the focus of the present paper would be on two issues: to analyze the influence of oxygen gas concentration (OGC) on the stoichiometry phase, and to study an effect of substrate temperature on the crystalline structure of tungsten oxide nanorods array. All samples have been characterized by using Raman spectra, scanning electron microscopy (SEM); energy dispersive X-ray spectroscopy (EDS), X-ray photoelectron spectroscopy (XPS) and X-ray diffraction (XRD) were also employed to characterize the samples.

Experimental Set Up

The nanostructured tungsten oxide materials were synthesized using a CVD technique. The Molybdenum (Mo) wafer was used as deposition substrate. Before placing the substrates in the CVD chamber, the mirror-like surface of the polished substrates were ultrasonically washed in a methanol solution for 5 min, rinsed with acetone, and dried with helium. After placing the substrate, the chamber was pumped down to 2.0×10^{-5} Torr before feeding the gases. Two kinds of gas mixture, 8.7% of CH_4, 0.3% O_2, and 91% H_2 and 8.3% of CH_4, 0.7% of O_2, and 91% H_2 gases were used. The flow rate of mixed gases was 5SCCM. The gas pressure inside the deposition chamber was maintained at

X. P. Wang · B. Q. Yang · H. X. Zhang · P. X. Feng (✉)
Department of Physics, University of Puerto Rico, P.O. Box 23343, San Juan, PR 00931, USA
e-mail: pfeng@cnnet.upr.edu

500 mTorr during the deposition. An AC power supply with electric current of 10 A and voltage of 8 V was used to heat the tungsten filament to temperature 2,400 °C to promote gas phase activation.

Results and Discussions

Figure 1 showed two SEM images of surfaces of the samples prepared under OGC of (a) 0.3% and (b) 0.7% in mixture gases at 400 °C for 1 h of deposition. Differences between the two surface structures were distinguishable. Generally, low OGC resulted in yielding nanoscale WO particles, which was shown in Fig. 1a. The particles uniformly distributed. The scale of the particles was similar, which was 1 μm around. The film's color looked like ivory-white, and its surface appeared glossy. Figure 1b showed the SEM image of the samples under high OGC. The sample's color was violet blue, which was the typical color of tungsten trioxide. The sample's surface was dim. It could be easily observed that the tungsten oxide rods arrayed very well. They were vertical to the substrate. The diameter of the rod was 400 nm averagely. The number of rods per unit area (Fig. 1b) was almost the same as the number of the total particles on the top surface of the sample (Fig. 1a). Therefore, it could be assumed that the particles on the top layer in sample (a) could be the base of the tungsten oxide rods shown in Fig. 1b. The particles on the bottom layer covered the substrate surface tightly, and then the top layer provided the seeds of the rods. If the OGC were high enough as the precursor, the tungsten oxide nanorods would keep yielding. If not, the nanorods would not exist. As mentioned above, the gas pressures of both experiments were kept nearly constant except slight variation of OGC from 0.3% to 0.7% in the gas mixture. Interest is that so little variation of OGC resulted in completely different WO_3 nanostructure.

Figure 2a, b showed the EDS of two tungsten oxide samples (Fig. 1a, b). The element component quantitative result was presented in Table 1. The EDS pattern in Fig. 2 indicated the sample not only consisted of tungsten and oxygen, but also some carbon atoms. The EDS signal (Fig. 2a) of oxygen was obviously weaker than that in Fig. 2b. This was in good agreement with the experimental conditions. From Table 1, it could be seen that variation of the oxygen concentration in the mixture gases in the chamber from 0.3% to 0.7% yielded oxygen component up to nearly 7% and 51%, respectively, inside the tungsten oxide samples. The ratio of atomic percentages between tungsten and oxygen was almost 9 under low OGC. In this case the phase of tungsten oxide supposed to be in sub-stoichiometry state. It could also be observed that the composition of carbon was remarkable which was even 4 times more than oxygen. On the other hand, under high OGC, the tungsten content decreased down to 38.66%, which was 20% lower than former one, whereas the component of oxygen largely increased up to 50%. Accordingly, the carbon component decreased rapidly, less than 20%.

Based on the data above, the stoichiometry variation can be given. As seen under low OGC, the carbon content inside the sample was higher than that of oxygen. Therefore, two possible chemical states might coexist inside the sample. One was tungsten oxide together with tungsten carbide. Due to lack of oxide component, the stoichiometry phase of tungsten oxide should be WO_{3-x}, where x was related to the stoichiometry phase of tungsten carbide. The second possibility was that carbon atoms, tungsten atoms, and tungsten oxide mixed but independently existed, which mean there were no chemical bonds among them. This expectation has been confirmed by XPS or XRD measurements below.

When the OGC in the mixture gases was high, the obtained oxygen content inside the sample was up to 50%. The percentage of the carbon inside the sample descended to 10%. Consequently, tungsten oxide dominated the sample. This was verified by using XPS. Figure 3a showed the tungsten peaks for the sample prepared under low OGC. Four peaks were observed at 37.97 eV, 35.87 eV, 33.38 eV and 31.2 eV. The typical doublet W4f peaks were clearly visible in the spectra, which were at 31.2 eV and 33.38 eV. The existence of these two peaks strongly

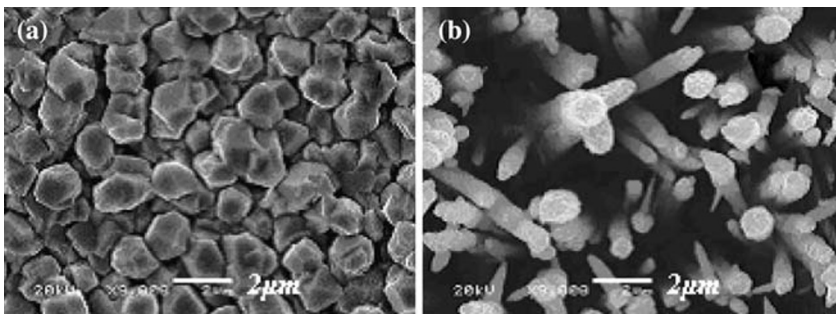

Fig. 1 SEM images of the samples prepared under (**a**) low OGC, and (**b**) high OGC

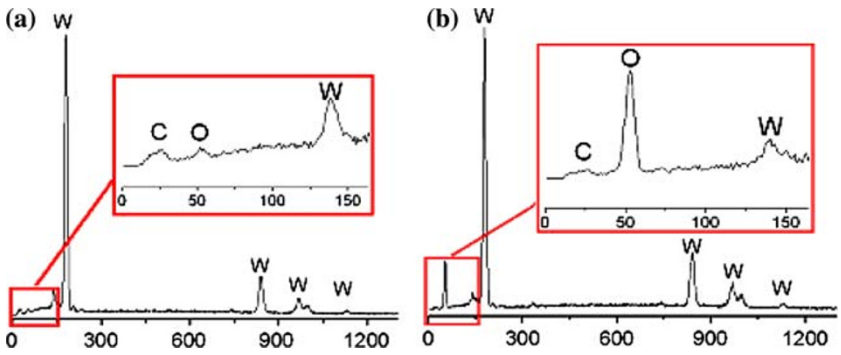

Fig. 2 EDS of the samples (Fig. 1) for (**a**) low and (**b**) high OGC

Table 1 EDS elements component quantitative results

	Low OGC		High OGC	
	Wt%	At%	Wt%	At%
W K	95.39	58.78	88.33	38.66
O K	0.95	6.72	10.07	50.63
C K	3.66	34.50	1.60	10.72

proved the assumption of deposition of atomic tungsten. The two upper binding energy peaks exhibited the presence of oxygen modified $W4f_{5/2}$ and $W4f_{7/2}$ status. It was also found that there was a shoulder at upper energy side of each atomic tungsten peak. By looking up the database of National Institute of Standard Technology (NIST), these shoulders were related to WO_2 and WO_x. No specified carbon modified tungsten peaks could be found in the XPS profiles of the samples. Considering the assumption of compound component mentioned above, it was concluded that atomic carbon, atomic tungsten and sub-stoichiometry tungsten oxide existed in this tungsten oxide particle-based thin film.

The XPS profile of sample (b) prepared under high OGC was shown in Fig. 3b. The oxygen modified tungsten features remained unchanged, indicating the presence of stoichiometry tungsten oxide. The peaks of atomic tungsten vanished. Moreover, the shoulder peaks related to WO_2 or WO_x also disappeared. This evidence strongly supported the stoichiometry phase evolution of the tungsten oxide.

Figure 4 showed the Raman spectra of the tungsten oxide samples related to Fig. 1a, b. Two broad but weak bands marked with K1 and K2 located in 770 cm^{-1} and 870 cm^{-1} which was shown in Fig. 4a, were related to tungsten oxide. Typical Raman peaks of crystalline tungsten oxide located at 700 cm^{-1} and 800 cm^{-1}. The shift resulted from the different chemical experimental conditions. In fact, such weak humps revealed that the obtained tungsten oxide particle-based film was in amorphous states.

Under high OGC, much more prominent Raman spectra peaks at 701 cm^{-1} and 801 cm^{-1} were indicated in Fig. 4b, which supported the existence of tungsten trioxide. A conclusion from Raman spectra was revealed: the crystalline tungsten oxide has been yielded under high OGC. Variation from the two weak humps in Fig. 4a to prominent peaks in Fig. 4b indicated that the crystalline structural evolution followed the change of OGC.

The XRD patterns of the samples were showed in Fig. 5. All four XRD peaks of the first sample shown in Fig. 5a were from tungsten components. From XPS, we have also known that the first sample included atomic tungsten component, WO_2 component, and WO_3 component. These results provided evidence again that the first sample was in amorphous status. It was in good agreement with the data obtained from Raman spectra. XRD pattern of the second

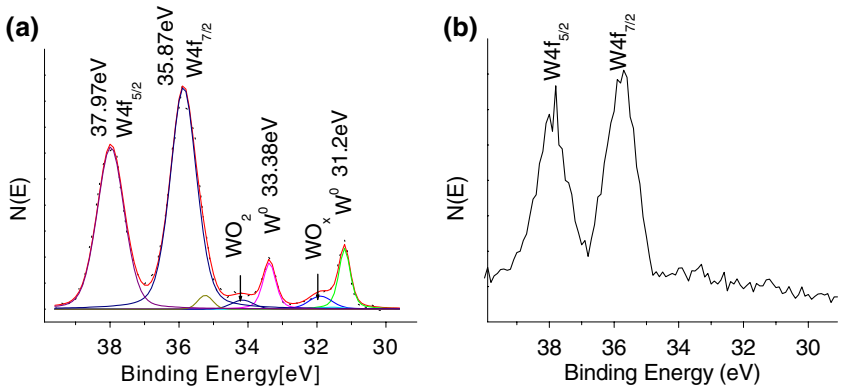

Fig. 3 XPS plot of (**a**) low OGC and (**b**) high OGC

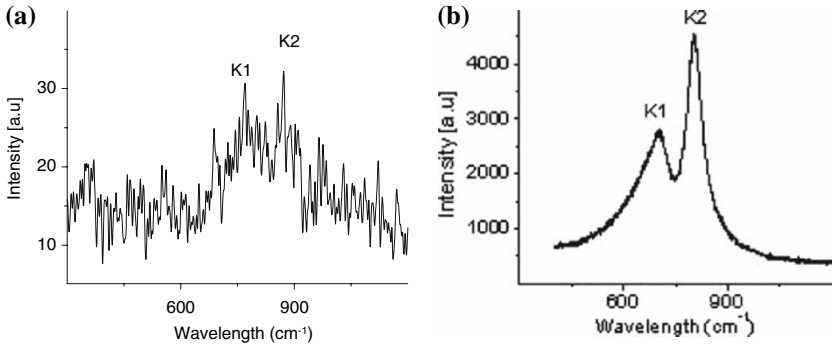

Fig. 4 (**a**) Raman profile for low OGC. (**b**) Raman profile for high OGC

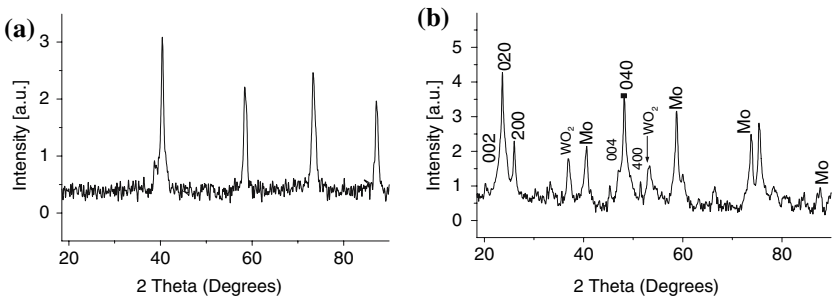

Fig. 5 (**a**) XRD pattern for low OGC. (**b**) XRD pattern for high OGC

sample shown in Fig. 5b was complicated. It included atomic tungsten, WO_2 and WO_3 XRD peaks. WO_3 XRD peaks dominated all spectral lines. The peaks marked as 002, 020 and 200, were related to monoclinic tungsten trioxide. The peak of crystalline orientations of 020 was much stronger than that of 200 and 002 orientations. Similar phenomenon was observed at the 2θ diffraction angles between 47° and 51°, which were associated with the orientations of 004, 040, and 400. Meanwhile, the peak of 040 was the strongest one. This fact showed that the polycrystalline tungsten trioxide of the sample was yielded, and the orientation of 020 dominated the trend of growth.

In summary, the stoichiometry phase evolution of tungsten oxide highly depended on the variation of OGC in mixture gases during deposition. Following an increase of OGC, the sub-stoichiometry tungsten oxide-WO_2 and WO_x-would become stoichiometry tungsten oxide. It was also found that atomic tungsten and carbon without any chemical bond structure would be mixed inside the sample. The variation of OGC also determined the structural evolutions from amorphous to crystal. Low OGC caused yielding amorphous tungsten oxide, whereas high OGC resulted in producing polycrystalline WO_3.

As a comparison, the effect of variation of substrate temperature on the sample nanostructure and chemical bond was also studied. Figure 6 shows SEM images of the samples prepared at substrate temperature of (a) 800 °C, (b) 1,000 °C and (c) 1,200 °C. All other conditions such as OGC in the mixture gas, gas pressure, gas flow rate, filament temperature and deposition duration were kept same as the sample shown in Fig. 1b.

The morphologies of these three samples were prominently different. The sample of tungsten oxide prepared at 800 °C (Fig. 6a) was thin, sharp and short. Nanobundle was generated in this sample. The diameter of single nanorod was around 200 nm, and the length was 2 μm. The nanobundle was so compact that it tended to yield to larger nanorod. The sample yielded at 1,000°C was shown in Fig. 6b. The hump-like nanostructured tungsten oxide was obtained. The diameter of the hump at this temperature was 500 nm approximately. It could be assumed that the nanobundle in Fig. 6a gathered then became a hump. This dynamic phenomenon was similar to the little drip gathering to be a larger drip. Furthermore, the tungsten oxide nanorod was clearly shown in Fig. 6c. The diameter of the nanorod was more than 500 nm, and the length was longer than 5 μm.

Based on these three samples, it was concluded that the growth rate of tungsten oxide increased following the rising of temperature, resulting in that the sample diameter was large and the length was long. Similar result was reported by Chi et al. [10] and Pal et al. [11]. It was especially mentioned that the root of each nanobundle was thinner than the main body [10]. So it could be inferred that the thin nanobundle at lower temperature could be the base of the sample prepared at higher temperature, which was similar to the condition shown at former paragraph concerning the different OGC.

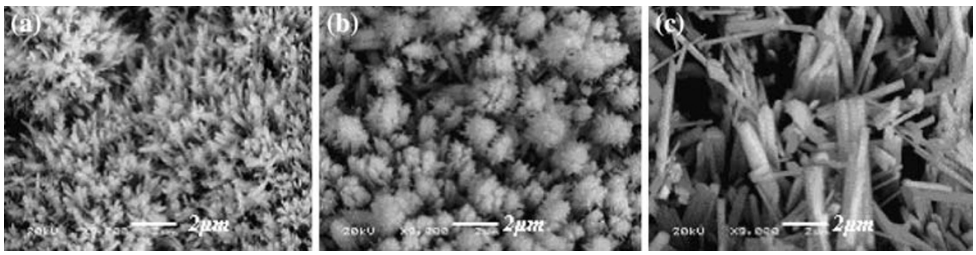

Fig. 6 SEM images for the samples at substrate temperatures of (**a**) 800 °C (**b**) 1,000 °C and (**c**) 1,200 °C

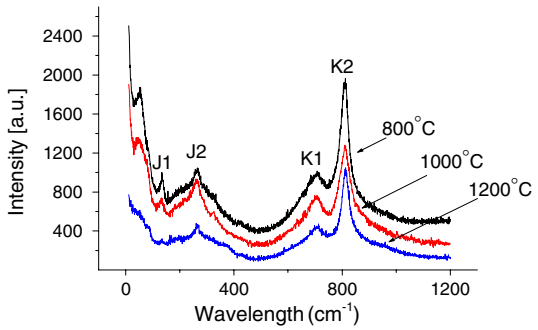

Fig. 7 Raman profiles for samples at different deposition temperatures

Figure 7 showed Raman profiles for these three samples (Fig. 6). Several Raman peaks were clearly visible, where peaks (signals) marked with J and K in the Raman profile, respectively. No shift existed for all these three spectra, which showed the structural stability of the samples at high temperature was very well. In general, the bands situated at around 700 and 800 cm^{-1} could be assigned to W–O stretching model, whereas the bands situated at around 130 and 270 cm^{-1} were associated to W–O bending modes of monoclinic WO_3 [12] Miyakawa has shown that the Raman bands at 809 and 718 cm^{-1} were for monoclinic WO_3 and did not change as a function of temperature (<500 °C), [13] indicating the formation of a highly stable monoclinic crystalline WO_3. The present data indicated that the stretching mode would not change even the temperature higher than 500 °C. However, the bending mode vanished at 1,200 °C. Therefore the bending mode was not as stable as stretching mode and it depended on the substrate temperature.

Conclusion

In conclusion, the variation of the properties of tungsten oxide highly depended on the OGC of the gas mixture. Slight rise of OGC from 0.3% to 0.7% in the mixture gas during deposition resulted in large change of the oxygen quantitative component in samples from 7% to 51%; the morphologies of the samples varied from particle-based film to nanorods array, and the chemical phase developed from sub-stoichiometry phase to stoichiometry. The crystalline structure also altered to crystalline tungsten oxide from amorphous structure. The sample prepared under high substrate temperature (800 °C–1,200 °C) was also investigated. The diameter and length of the samples' nanostructure grew up by raising the substrate temperature. The evolution of morphology was prominent, whereas the structure was quite stable. Based on the evidences above, it could be concluded that the properties of tungsten oxide were highly sensitive to the experimental parameters during deposition, especially the OGC in the gas mixture.

Acknowledgements This work has been supported by NSF-EPSCoR and DoD grants. We would like to thank Mr. William's assistance of Raman measurements, Mr. Ortiz and Ms. Hernandez for SEM and EDS measurements, Mr. Esteban for XPS measurements and Mr. Wu for XRD measurements.

References

1. P. Poizot, S. Grugeon, L. Dupont, J.-M. Tarascon, Nature **407**, 496 (2000)
2. C. Julien, E. Haro-Poniatowski, M.A. Camacho-Lòpez, L. Escobar-Alarcòn, J. Jimenez-Jarquin, Mater. Sci. Eng. B **65**, 170 (1999)
3. M. Ponzi, C. Duschatzky, A. Carrascull, E. Ponzi, Appl. Catal. A **169**, 373 (1998)
4. C.G. Granquist, *Handbook of Inorganic Electrochromic Materials*. (Elsevier Science, Amsterdam, 1995)
5. A. Talledo, C.G. Granqvist, J. Appl. Phys. **77**, 4655 (1995)
6. J. Livage, Chem. Mater. **3**, 758 (1991)
7. G. Micocci, A. Serra, A. Tepore, S. Capone, R. Rella, P. Siciliano, J. Vac. Sci. Technol. A **15**, 34 (1997)
8. F. Galléa, Z. Li, Z. Zhang, Appl. Phys. Lett. **89**, 193111 (2006)
9. C. Klinke, J.B. Hannon, L. Gignac, K. Reuter, P. Avouris, J. Phys. Chem. B **109**, 17787 (2005)
10. L. Chi, N. Xu, S. Deng, J. Chen, J. She, Nanotechnology **17**, 5590 (2006)
11. S. Pal, C. Jacob, Appl. Surf. Sci. **253**, 3317 (2007)
12. Z. Lu, S. Kanan, C. Tripp, J. Mater. Chem. **12**, 983 (2002)
13. K. Nonaka, A. Takase, K. Miyakawa, J. Mater. Sci. Lett. **12**, 274 (1993)